Design and Verification for the Torque Improvement of a Concentrated Flux-Type Synchronous Motor for Automotive Applications

Jong-Hyun Park, Kyung-Tae Jung, Young-Hoon Jung, Myung-Seop Lim, Myung-Hwan Yoon, Jung-Pyo Hong, *Senior Member, IEEE*, and Jae-Woo Jung

***Abstract*—In this paper, the design of the concentrated flux-type synchronous motor (CFSM) using ferrite permanent magnets to improve torque is proposed for an automotive chassis actuator. The thin pancake type CFSM of this paper has considerable axial magnetic leakage flux due to structural reasons. It is, therefore, necessary to improve the torque. In order to meet the required specifications in a constrained installation space, this paper proposes two methods for torque improvement. The first method is the alternate-stacking core as this structure removes the magnetic leakage flux path. The second method is the rotor overhang that increases the air-gap flux density. Furthermore, the structures require a three-dimensional (3-D) finite element method (FEM) analysis for accuracy. However, to analyze the characteristics easily and quickly, the 3-D structure is made into the equivalent 2-D FEM through an analytical method using an equivalent magnetic circuit. Finally, in this paper, the validity of the design process and the effectiveness for torque improvement is verified through experiments.**

***Index Terms*—Alternate-stacking cores, automotive chassis actuator, axial magnetic leakage flux, concentrated flux-type synchronous motor (CFSM), equivalent magnetic circuit (EMC), ferrite permanent magnet (PM), rotor overhang, shape ratio (SR), torque improvement, two-dimensional (2-D) equivalent method.**

Manuscript received June 5, 2018; revised September 22, 2018, December 24, 2018, and February 26, 2019; accepted March 14, 2019. Date of publication March 18, 2019; date of current version June 29, 2019. Paper 2018-EMC-0477.R3, presented at the 2017 IEEE International Electric Machines and Drives Conference, Miami, FL, USA, May 21–24, and approved for publication in the IEEE TRANSACTIONS ON INDUSTRY APPLICATIONS by the Electric Machines Committee of the IEEE Industry Applications Society. *(Jong-Hyun Park and Kyung-Tae Jung contributed equally to this work.) (Corresponding author: Jae-Woo Jung.)*

J.-H. Park is with the Traction Motor Engineering Design Team, Hyundai Transys, Hwaseong 18280, South Korea (e-mail: pjh@hyundaitransys.com).

K.-T. Jung, Y.-H. Jung, and J.-P. Hong are with the Automotive Engineering, Hanyang University, Seoul 04763, South Korea (e-mail: ktjung8310@hanyang.ac.kr; yhjung207@hanyang.ac.kr; hongjp@hanyang.ac.kr).

M.-S. Lim is with the School of Mechanical Engineering, Yeungnam University, Gyeongsan 38541, South Korea (e-mail: limmang87@yu.ac.kr).

M.-H. Yoon is with the Electric Power Drivetrain Engineering Design Team, Hyundai-Kia Motors, Hwaseong 18280, South Korea (e-mail: myunghyoon@gmail.com).

J.-W. Jung is with the Advanced Brake Engineering Team, Hyundai Mobis, Yongin 16891, South Korea (e-mail: jjwoo@mobis.co.kr).

Color versions of one or more of the figures in this paper are available online at http://ieeexplore.ieee.org.

Digital Object Identifier 10.1109/TIA.2019.2906296

I. Introduction

RECENTLY, the automobile industry has seen an increased emphasis on both vehicle safety and the environment. Improvement in automotive technology has contributed greatly to the safety of vehicles and the environment. Increased functionality has resulted in products such as electric power steering (EPS), anti-lock brake system (ABS), adaptive front lighting system (AFLS), electronic stability control (ESC), and the automotive chassis application assist system. Furthermore, in an effort to continue this improvement in functionality and reduction in both environmental pollution and vehicle accidents, automotive component manufacturers and car manufacturers are developing electro-mechanical systems. This has resulted in a demand for electric motors increasing significantly for automotive parts such as a hybrid system, brake, and turbocharger [1]–[4]. There are various types of permanent magnet synchronous motors (PMSM) applied to many automotive chassis applications, such as EPS, ABS, AFLS, ESC, the electric booster, etc. Recently, the majority of motors in automotive applications actuator use a surface-mounted permanent magnet synchronous motor (SPMSM) because it is relatively small in size and has a simple rotor structure. However, the SPMSM designed for the automotive application usually has a retainer in the rotor to prevent the scattering of the permanent magnet (PM). This additional structure increases the volume, weight, and magnetic air-gap. To overcome such a disadvantage of the SPMSM, on improving torque characteristics and optimizing the design of the interior permanent magnet synchronous motor (IPMSM) has been researched [5]–[11]. Furthermore, the IPMSM that uses the rare-earth PMs has attracted attention for its high-power density which is greater than that of the SPMSM, and because it can use the magnetic and reluctance torque with the current phase control method [12], [13]. However, the prices of the rare-earth PMs have increased, and there are concerns about the stability of the raw material supply for Neodymium and Dysprosium. In severe cases, exports have been limited. Therefore, the use of rare-earth PMs should be reduced [14]–[19]. To reduce the dependence on rare-earth PMs, various motors without the rare-earth PM, such as induction motors, synRMs, and concentrated flux-type synchronous motor (CFSM), have entered development. Among the many various motors without the rare-earth PMs, the CFSM that uses ferrite PM is one of the most effective. However, the

TABLE I
INSTALLATION SPACE AND SPECIFICATIONS OF MOTOR

Parameter	Unit	Value
Stator outer diameter	mm	75
Stack length	mm	22.5
Rated torque	Nm	1.7
Rated speed	rpm	3,300
Line to line voltage (rms value)	V	7.34
Limit current (rms value)	A	65
Connection	-	Delta

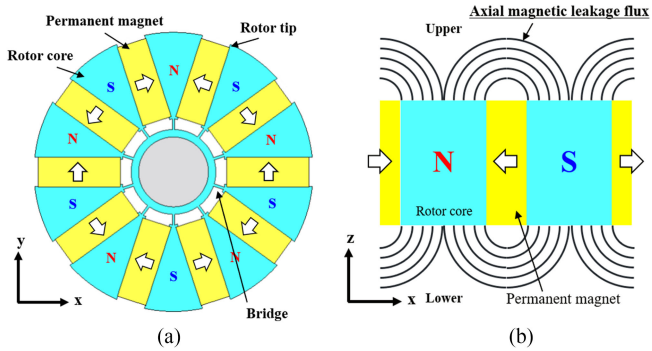

Fig. 1. Axial magnetic leakage flux of CFSM. (a) Geometry of CFSM. (b) Axial magnetic leakage flux path.

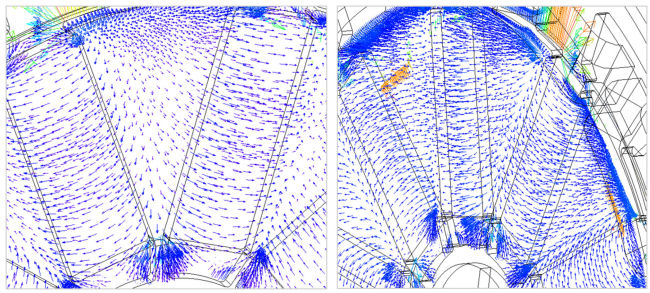

Fig. 2. Axial magnetic leakage flux of CFSM through 3-D FEM.

residual induction of the ferrite PMs is one-third of that of the rare-earth PMs. On the other hand, the cost of the ferrite PMs compared to the rare-earth PMs is about one-tenth and the stable supply of the ferrite PMs is readily available. As previously mentioned, due to the low residual induction of the ferrite PMs, it is necessary to increase the amount of ferrite PM so as to satisfy the performance in terms of both power and torque [14]–[23]. This means an increase in the motor size.

In contrast, as the automotive industry becomes ever more sophisticated, there is an increasing demand for CFSMs with a short axial length and that are able to use more ferrite PMs. The shape of this motor resembles that of a thin pancake. A disadvantage of these thin pancake CFSMs is the axial magnetic leakage flux. Because of this drawback, CFSMs designed in the form of a thin pancake degrade performance at the same volume. Thus, while volume increase is essential to satisfy the equivalent performance, the installation space for the vehicle is constrained. Previous research related to the CFSM using the ferrite PMs did not take the installation space and specifications into consideration, while the automotive actuator was required to meet the output power in a constrained installation space. The installation space of the actuator used in this study is shown in Table I. Therefore, this paper proposes a method and a process for improving the torque. The first method is the alternate-stacking core and this structure removes the magnetic leakage flux path. The second method is the rotor overhang and this structure increases the air-gap flux density. Those structures require a three-dimensional (3-D) finite element method (FEM) for accurate analysis. However, to analyze the characteristics more easily and quickly, the 3-D structure is made into the equivalent 2-D FEM. Finally, in this paper, the validity of the torque improvement methods is verified through load tests.

II. AXIAL MAGNETIC LEAKAGE FLUX

A. Axial Magnetic Leakage Flux Effect

Fig. 1(a) shows the rotor structure of the CFSM. As shown in Fig. 1(a), the rotor core is separated by the PM. The magnetic flux of the PMs arranged on both sides is concentrated and magnetized to the rotor core. Therefore, the adjacent rotor cores are magnetized to different poles. The magnetized rotor core is only connected to the magnetically saturated bridges. Magnetically saturated bridges and PMs have similar permeability. As a result, different polarities are magnetized in the neighboring rotor core, so that axial magnetic leakage flux occurs as shown in Fig. 1(b) [24]. Moreover, Fig. 2 demonstrates the axial magnetic leakage flux path can be confirmed through 3-D FEM.

B. Axial Magnetic Leakage Flux With Shape Ratio (SR)

The aforementioned problem of the CFSM is that there is a magnetic leakage flux to the other pole of the adjacent rotor core without concentrated magnetic flux being transmitted to the stator via the air-gap. More specifically, as the SR representing the ratio between the outer diameter of the rotor and the stack length is lower, the no-load Back Electromotive Force (BEMF) tends to decrease due to the increase in the magnetic leakage flux, as shown in Fig. 3. Where SR is defined as follows:

$$\mathrm{SR} = \frac{L_{\mathrm{stk}}}{D_{\mathrm{r}}} \tag{1}$$

where D_{r} is the rotor diameter and L_{stk} is the stack length.

As shown in Fig. 3, the no-load BEMF of the CFSM and the SPMSM decreases as the SR lowers. When the pancake type (SR <1) with a thinner stacking length than the rotor diameter becomes, so that the influence of the magnetic leakage flux becomes larger, the no-load BEMF decreases. At the same SR ($=0.3$), the decrease in the no-load BEMF due to the axial magnetic leakage flux of the CFSM is four times greater than the decrease in the SPMSM. The relation between the no-load BEMF and the mechanical power can be expressed by (2) based on the energy conservation law. If the input current and mechanical angular velocity are constant, the no-load BEMF and the torque

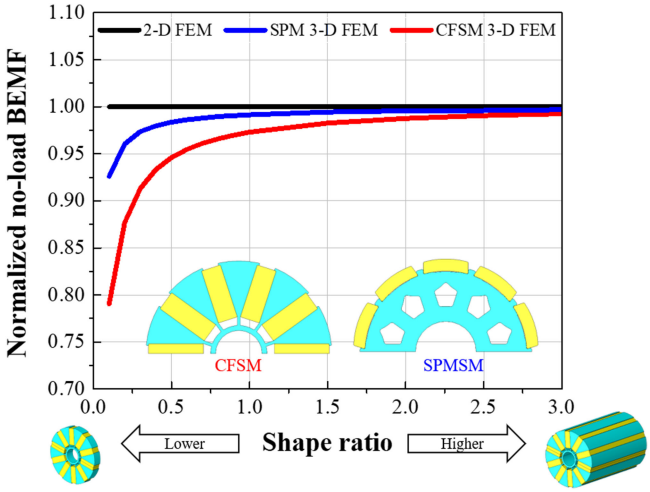

Fig. 3. Normalized no-load BEMF according to shape ratio.

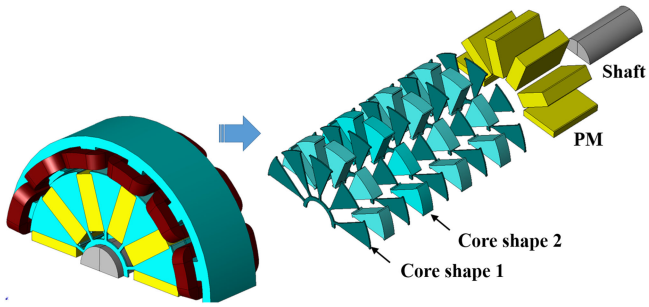

Fig. 4. CFSM structure of alternate-stacking cores and rotor overhang.

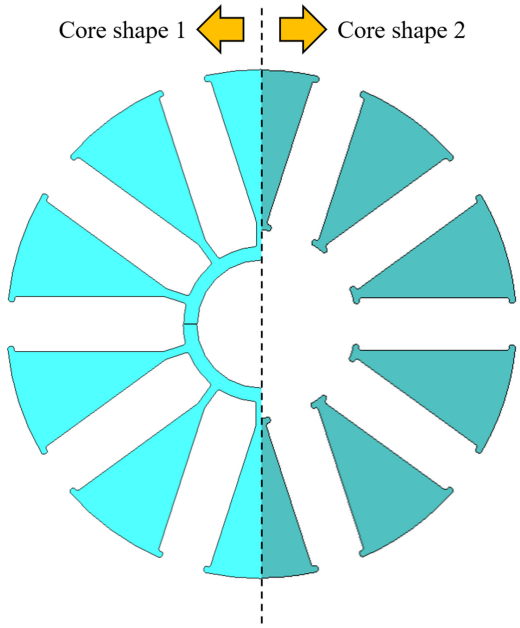

Fig. 5. Alternate-stacking cores of two shape.

are proportional. Therefore, the torque of the CFSM is lower than that of the SPMSM as the BEMF decreases due to the axial magnetic leakage flux

$$\omega_{\mathrm{m}} T = mei \tag{2}$$

where ω_{m} and T are the mechanical angular speed and torque, respectively. m is the number of phases. e is the no-load BEMF. i is the input current.

In summary, the CFSM has a considerably large axial magnetic leakage flux that does not pass through the air-gap for the structural reasons discussed above. In particular, the CFSM with a low SR should consider torque reduction due to axial magnetic leakage flux. This paper thus proposes torque improvement methods to compensate for the torque reduction due to the axial magnetic leakage flux and meet the desired performance in the constrained installation space.

III. Methods for Torque Improvement

Previous research work related to the CFSM using ferrite magnets did not consider either the installation space or the specification. The designed motors did not face space constraints. However, the automotive applications should meet the torque in a constrained installation space and specification. Those of the automotive application motor used in this study are shown in Table I. Here, the SR of the automotive application motor should be less than 1 due to the restricted installation space. (In practice, SR = about 0.3).

A. Torque Improvement Method

There are many methods capable of improving torque [14]–[29]. The methods in [14], [15], [20], [28] and [16], [21] have improved torque using a PM-assisted motor and axial gap motor, respectively. The methods in [17]–[19], [22], [24], and [26] increased the torque using CFSM and dual-stator. The optimal design has been conducted to improve the torque in [23] and [25]. In [27], the torque is improved from the control point of view. The method in [29] improved the torque performance by applying the magnetic leakage reduction structure. Among the various methods, this paper proposes two methods that are able to increase torque in a constrained installation space and then discuss how to apply them to rotor design. The first method is to apply an alternate-stacking core of two-shapes as shown in Fig. 4. The alternate-stacking core consists of two different rotor core shapes. More specifically, core shape 1 is a general CFSM rotor core, and core shape 2 removes the bridge shaft side which is the main magnetic leakage flux path as shown in Fig. 5. The advantage of the alternate-stacking core of two-shapes is that they can be alternately stacked at an appropriately selected ratio to reduce magnetic leakage flux. Second, the rotor overhang is applied to increase the usage of PMs as shown in Fig. 6. The rotor overhang means that the stack length of the rotor, including the PMs, is longer than that of the stator. The advantage of this structure is to increase the air-gap magnetic flux density [30], [31].

Unfortunately, both the above-proposed methods have a 3-D magnetic field distribution and the characteristics of the motor can be confirmed by 3-D FEM. In other words, the two proposed methods capable of improving the torque do not have

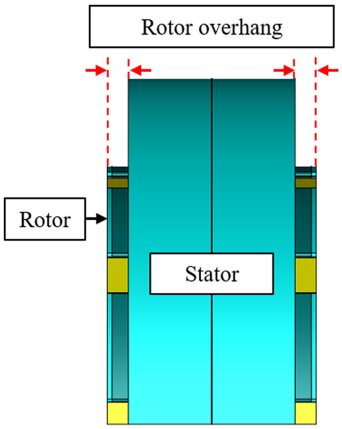

Fig. 6. Rotor overhang including the PMs.

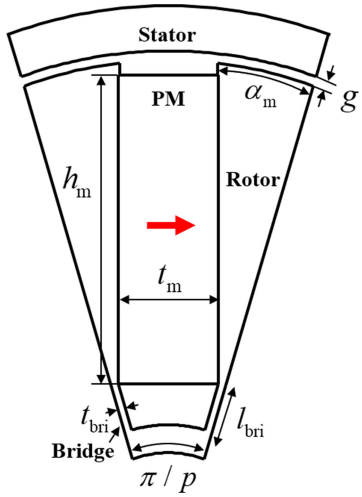

Fig. 7. Geometry of the CFSM.

a symmetrical structure in the axial direction (z-direction) as shown in Fig. 4. The 3-D FEM provides precise simulation results. However, the 3-D FEM is not an effective solution because of the tremendous computation costs. Moreover, it has a complicated preprocessing method, including geometry and mesh modeling [30]–[32]. It is also difficult to confirm the torque and various characteristic tendencies according to the motor parameters. Therefore, in this paper, we propose a method to evaluate the tendency of the 3-D magnetic field distribution with the 2-D FEM, and we will use this to reflect the design of the rotor.

B. 2-D FEM Analysis Considering Alternate-Stacking Core

In the 2-D FEM analysis, only the magnetic flux in the x- and y-direction can be considered in the analysis. However, the alternate-stacking cores of two-shapes are not uniform and unsymmetrical in the axial direction (z-direction). It is not applicable in a typical 2-D FEM and is therefore considered for the 3-D FEM. However, to solve the problem of the 3-D FEM, this paper proposes a method of equalizing the 3-D FEM with 2-D FEM using an equivalent magnetic circuit (EMC). For this analytical approach, the simplified geometry of the CFSM is shown in Fig. 7. The EMC taking into consideration the bridges are shown in Fig. 8. The EMC used in this paper applies the same assumptions available in previous work [17].

In Fig. 7, g is the air-gap length in mm. p is the number of pole-pair. $\alpha_{\rm m}$ is half of pole arc in radian. $t_{\rm m}$ and $h_{\rm m}$ are the thickness and height of the PM in mm, respectively. $l_{\rm bri}$ and $t_{\rm bri}$ are the length and the thickness of the bridge in mm, respectively.

In order to equalize the 2-D FEM and 3-D FEM, two types of EMC are designed and compared. The first EMC is a 2-D EMC, and the second EMC is a 3-D EMC. The meaning of the 2-D EMC means to stack only 1 core shape continuously, whereas the 3-D EMC means to alternate-stacking cores of core shape 1 and 2.

The characteristics of the motor have a considerable effect on the magnetic flux density in the air-gap. Similarly, the air-gap magnetic flux density should be the same in the 2-D and the 3-D EMC. The relationship between magnetic flux density and

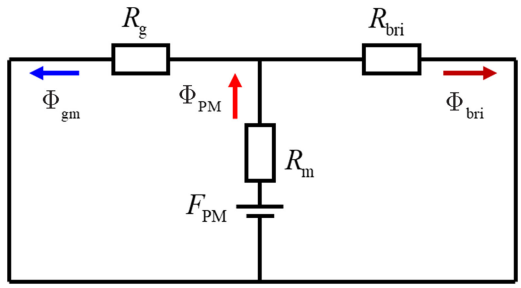

Fig. 8. EMC considering the bridges.

magnetic flux is shown in the following equation:

$$\vec{B} = \mu \vec{H} \tag{3}$$

where B and H are the magnetic flux density in T and the magnetic field intensity in A/m, respectively. μ is the permeability in H/m. And the air-gap magnetic flux $\Phi_{\rm gm}$ of EMC can be expressed by (4) according to the Gauss's law

$$\Phi_{\rm PM} = \Phi_{\rm gm} + \Phi_{\rm bri} \tag{4}$$

where $\Phi_{\rm PM}$ and $\Phi_{\rm bri}$ are the magnetic flux of PM in Wb and the magnetic flux of bridge in Wb, respectively. $F_{\rm PM}$ is the magnetomotive force of the PM. $R_{\rm m}$ is the magnetic reluctance of the PM in A/Wb. $R_{\rm bri}$ and R_g are the magnetic reluctance per one pole of the bridge and the air-gap in A/Wb, respectively.

In (4), it is possible to equalize the 2-D EMC and 3-D EMC by making the air-gap flux the same. That is, if the 2-D EMC and 3-D EMC have the same amount of magnetic flux in the PMs and the same magnetic leakage flux in the bridge, the air-gap flux density is the same. As a result, for the magnetic leakage flux of the 2-D EMC and the 3-D EMC to be the same, the reluctance expressed by the geometric dimensions should be the same. The same reluctance of the 2-D EMC and the 3-D EMC is expressed by the following equation:

$$\frac{l_{\rm bri\_3D}}{\mu_0 \mu_r t_{\rm bri\_3D} L_{\rm stk\_bri}} = \frac{l_{\rm bri\_2D}}{\mu_0 \mu_r t_{\rm bri\_2D} L_{\rm stk\_total}} \tag{5}$$

where $l_{\mathrm{bri\_3D}}$ and $l_{\mathrm{bri\_2D}}$ are the bridge length of 3-D and 2-D, respectively. μ_0 and μ_r are the air permeability and relative permeability, respectively. $t_{\mathrm{bri\_3D}}$ and $t_{\mathrm{bri\_2D}}$ are the 3-D bridge thickness and 2-D bridge thickness, respectively. $L_{\mathrm{stk\_bri}}$ and $L_{\mathrm{stk\_total}}$ represent the stack length of core shape 1 and total stack length of rotor cores, respectively.

Equation (5) can be rearranged to derive (6). In conclusion, it can be concluded that the alternate-stacking cores can be equalized through the bridge thickness of the 2-D FEM

$$t_{\mathrm{bri\_2D}} = t_{\mathrm{bri\_3D}} \frac{L_{\mathrm{stk\_bri}}}{L_{\mathrm{stk\_total}}} \tag{6}$$

The bridge thickness of the 2-D FEM model can be verified by (6). $t_{\mathrm{bri\_2D}}$ represent the 2-D FEM bridge thickness in mm. Therefore, the alternate-stacking cores that need to be verified by 3-D FEM can be replaced by 2-D FEM.

C. Rotor Overhang for Torque Improvement

In this paper, the second method capable of improving the torque in a constrained installation space is to apply the rotor overhang as shown in Fig. 6. The rotor overhang structure also requires a 3-D FEM analysis as did the alternate-stacking core structure. However, the proposal of this paper is to reflect the rotor overhang including the PMs at 2-D FEM. The PM's residual induction of the 2-D FEM is then modified by increasing the ratio of the 2-D FEM no-load BEMF to the 3-D FEM. Although the on-load has a significant influence on the characteristic of the motor, the air-gap flux density, which has a significant effect on the output torque, has a direct effect on the no-load BEMF. Therefore, preliminary prediction can be made based on the no-load BEMF as the open-circuit result. It is, therefore, reasonable to make a prediction based on the ratio according to (2).

For the 2-D FEM analysis, the modified residual induction of the PM that reflects the rotor overhang is given by the following equation:

$$B_{\mathrm{2D}} = B_r \frac{e_{\mathrm{1st\_rms\_3D}}}{e_{\mathrm{1st\_rms\_2D}}} \tag{7}$$

where B_{2D} and B_r are the modified residual induction of the 2-D FEM PM in T and the residual induction of the PM in T, respectively. $e_{\mathrm{1st\_rms\_3D}}$ and $e_{\mathrm{1st\_rms\_2D}}$ are the fundamental no-load phase BEMF of 3-D FEM considering the axial magnetic leakage flux in V and the fundamental no-load phase BEMF of 2-D FEM in V, respectively.

To verify the validation of the proposed equivalent method, the 3-D FEM and the equivalent 2-D FEM are compared in Fig. 9. The no-load BEMF of the 3-D FEM and equivalent 2-D FEM according to the stack ratio is compared because the no-load BEMF is the main characteristic of the motor. The stack ratio is the ratio of the length of the core shape 1 to the total length of the rotor. The stack ratio of 0 means that it is only composed of core shape 2, whereas the stack ratio of 1 means that it consists of core shape 1 only. As shown in Fig. 9, the results of the equivalent 2-D FEM are similar to those of the 3-D FEM. Therefore, it is confirmed that the proposed equivalent method is valid. The proposed method is also an effective method because it can confirm the results faster than the 3-D FEM.

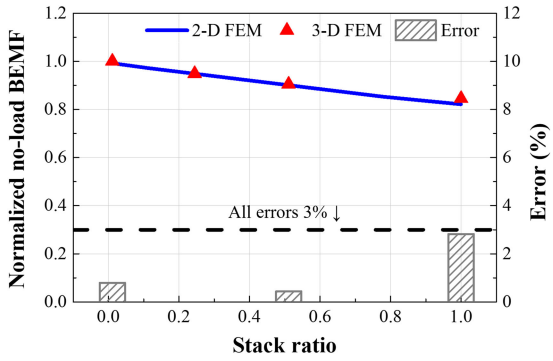

Fig. 9. No-load BEMF of the 3-D FEM and equivalent 2-D FEM according to the stack ratio.

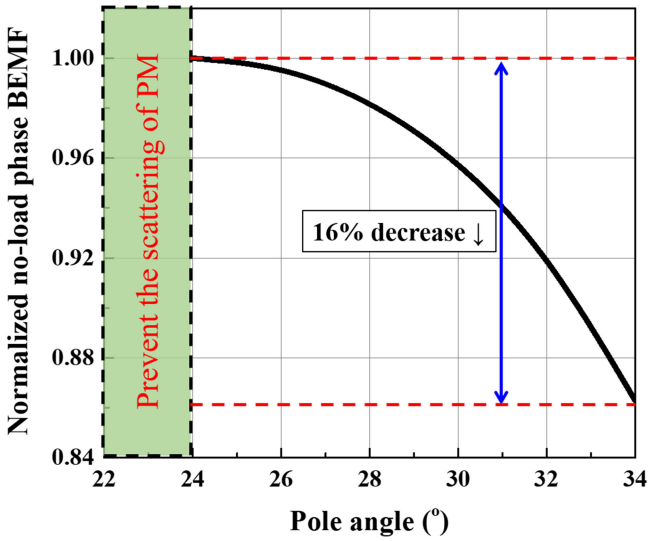

Fig. 10. Fundamental component of no-load phase BEMF tendency according to pole angle.

D. Pole Angle Determination

The rotor tips of the air-gap side are necessary to prevent scattering of PMs due to centrifugal force. The rotor tips are shown in Fig. 1. The rotor tips are important for the mechanical properties as well as for the torque characteristics of motors. The circumferential length of the rotor tips at both ends of the magnetized rotor iron core is defined as the pole angle. As mentioned above, the no-load BEMF is related to the torque of the motor. Therefore, the no-load BEMF tendency according to the change of the pole angle is shown in Fig. 10. The minimum of the pole angle is 24° to prevent the scattering of the PMs. As shown in Fig. 10, the BEMF increases as the polar angle decreases. In other words, the torque of the CFSM is better with the smaller pole angle. In conclusion, the pole angle was finally chosen at 26°, as the PMs and rotor tips had to make sufficient contact for mechanical stability reasons. The configuration of the motor is shown in Fig. 11.

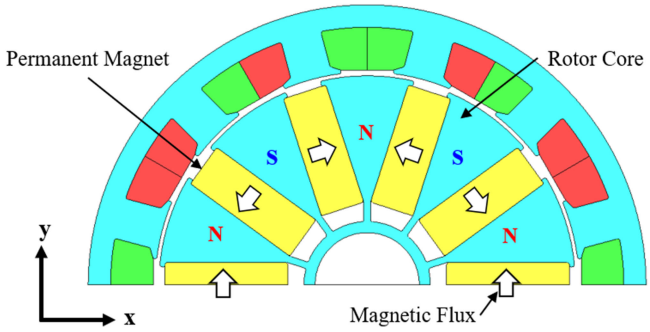

Fig. 11. Configuration of the designed motor.

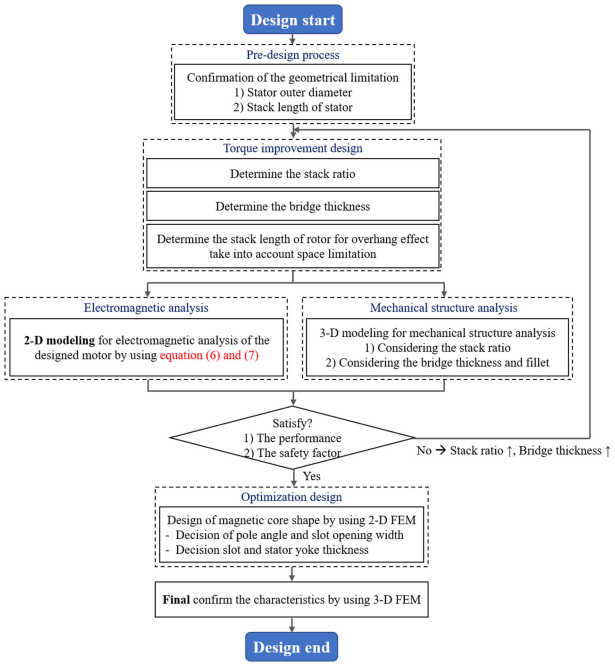

Fig. 12. Design process for improving the torque density in a constrained installation space.

IV. Verification

A. Specifications of Designed Motor

The rotor was designed by the above-mentioned equivalent method of the alternate-stacking core and rotor overhang. The important design variables are the bridge thickness and the stack ratio. The bridge thickness and stack ratio are determined by taking into consideration the mechanical strength and electric characteristics. Fig. 12 is the design process for improving the torque density in a constrained installation space. In the pre-design process, the outer diameter and the stack length of the stator are selected considering the space where the motor can be installed. Then, the methods of the torque improvement proposed in this paper are applied. Next, the electrical and mechanical characteristics are considered simultaneously. To quickly and easily examine the electrical characteristics of the motor applied the proposed method, the 3-D model is equivalent to the 2-D model using (6) and (7). The 2-D electromagnetic FEM is

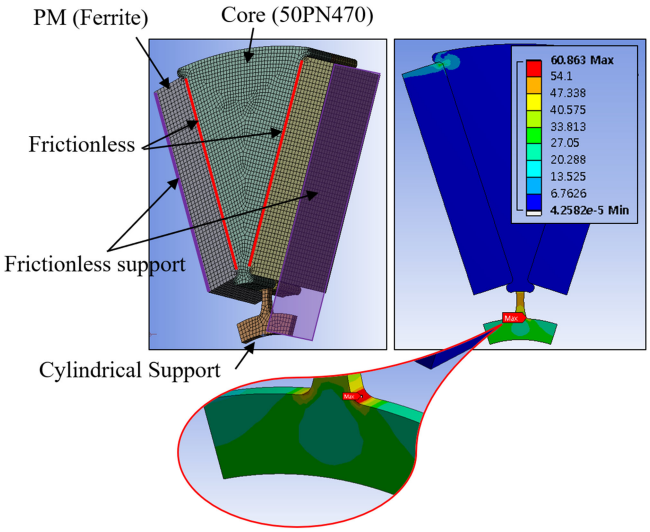

Fig. 13. Result of structural analysis by centrifugal force of the designed motor.

performed using the equivalent 2-D model. On the other hand, the mechanical characteristics are analyzed through 3-D mechanical FEM analysis considering the bridge thickness and the stack ratio. As a result, the bridge thickness is determined as 0.9 mm considering the mechanical strength and the manufacturable minimum thickness. The stack ratio is designed to be about 0.1 which is also the manufacturable minimum stack ratio. This stack ratio consists of the core shape 1 in 5 sheets and the core shape 2 in 40 sheets. Fig. 13 shows the result of structural analysis by the centrifugal force of the designed motor. The structural analysis is conducted on 1.2 times the maximum rotation speed and the material properties are shown in Table II. Since the same rotor structure is repeated along the direction of the stack length, it is used to analyze only the repeated minimum structure to reduce the analysis time. As shown in Fig. 13, the maximum stress is applied to the bridge and is about 60.9 MPa. Therefore, the safety factor of the designed motor is 4.5, which is considered stable enough. The safety factor of the proposed model applying the calculated bridge thickness and the stack ratio is 4.5, which is considered stable enough. In the alternate-stacking method, core shape 1 is evenly arranged to withstand the centrifugal force of the PM and core shape 2 as shown in Fig. 4.

It is clear in Table I that the stack length of the installation space is constrained to 22.5 mm. Thus, the stack length of the stator is selected as 18 mm considering the end turn height of the coils. As a result, the rotor stack length applying the rotor overhang is selected as 22.5 mm, the maximum available length. The rotor overhang structure can be seen in Fig. 6. The motor was driven via $I_{\mathrm{d}} = 0$ control. The detailed specifications of the CFSM are shown in Table III.

B. Verification of Designed Motor

To verify the validity of the equivalent method of the alternate-stacking core and rotor overhang, the designed model was set up,

TABLE II
MATERIAL PROPERTIES FOR STRUCTURAL ANALYSIS

	Unit	Core (50PN470)	PM (Ferrite)
Density	kg/m^3	7,700	5,100
Young's Modulus	GPa	180	150
Poisson's Ratio	-	0.30	0.25
Yield Point	MPa	275	276

TABLE III
SPECIFICATIONS OF DESIGNED MOTOR

Parameter	Unit	Value
Stator slot / Rotor pole	-	12 / 10
Stator outer diameter	mm	75
Stack length (stator / rotor)	mm	18 / 22.5
Bridge thickness	mm	0.9
Stack ratio	-	0.1
Rotor outer diameter	mm	56
Air-gap length	mm	0.5
Pole angle	°	24
PM size	mm^2	16.5 × 6
PM residual induction (NMF-9G)	T	0.41
The number of series turns per phase	-	34

and an experiment was conducted. The prototype of the designed motor is shown in Fig. 14. The specifications of the designed motor that fulfilled the requirements are shown in Table III.

In this paper, we compare and verify the original motor with the designed motor. Here, the original motor does not apply the torque improvement method proposed in this paper. However, the designed motor does apply the torque improvement method proposed in this paper.

In addition, the proposed 2-D equalization method was applied to verify the characteristics of the designed motor. Through this, the 2-D equivalent method is thus verified. The no-load BEMF, which has a significant effect on the characteristics of the motor, is compared and shown in Fig. 15.

As shown in Fig. 15, it is confirmed that the amplitude of the no-load BEMF waveform of the designed motor is larger than that of the original motor. In addition, the FEM analysis result of the designed motor is seen to be almost equal to the test. Specifically, when comparing the rms value of the fundamental of each waveform, the original motor is 1.51 V, the FEM result of the designed model is 1.81 V, and the experimental result is 1.73 V at 1000 r/min. As a result, the no-load BEMF of the model designed by the original motor is increased by 16.6%, and the error between the FEM analysis result and the test of the designed model is 4.6%. Through this, we indirectly confirmed the validity of the proposed method and the method capable of improving the characteristics of the motor by the method proposed in this paper.

Second, the torque test results were compared in the same way as the no-load BEMF and the test results are recorded in Fig. 16.

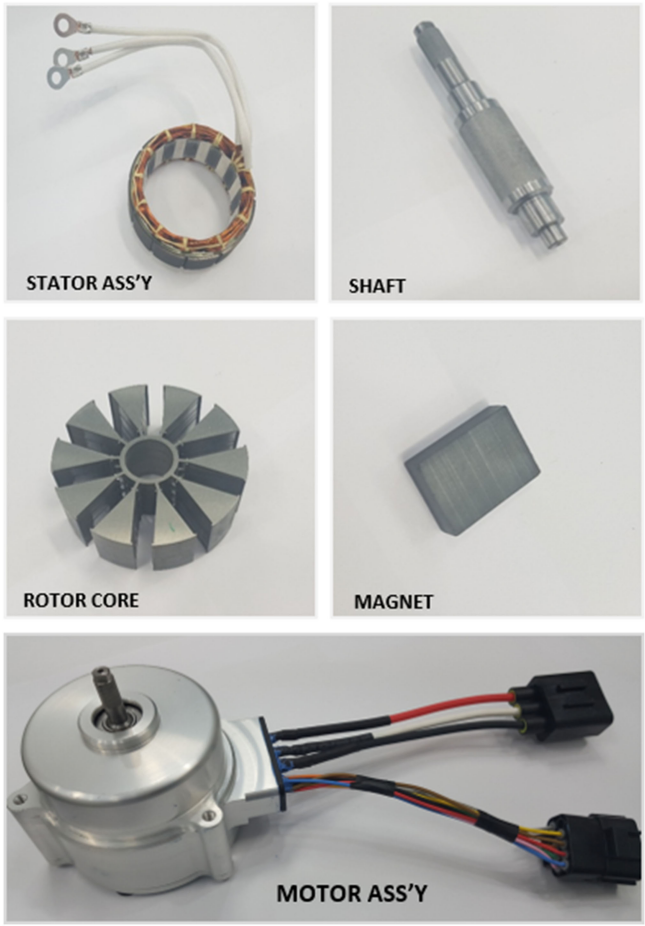

Fig. 14. Prototype of designed motor.

The motor was driven via $I_{\mathrm{d}} = 0$ control. As shown in Fig. 16, the torque according to each input current is compared. It was confirmed that the torque of the designed motor was increased more than that of the original motor, whereas the FEM analysis results and experimental results were confirmed to be almost the same. Specifically, the torque was confirmed at a limited input line current of the rms value 65 A and rated speed 3300 r/min. The original motor is 1.51 N·m, the FEM result of the designed motor is 1.75 N·m, and the test result is 1.76 N·m. As a result, the motor using the method for improving the torque has improved about 10% torque compared with the original motor. The FEM analysis results and the test result show an error of 0.6%.

Finally, we compared the torque, the core loss, copper loss, and efficiency of the original motor with the designed motor under the same input current conditions. The core loss analysis is based on the 3-D FEM. The volume of the bridge and the rotor yoke is reduced by 86% compared with that of the original model, while the core loss increases by only 1 W in comparison to the original motor. Because the percentage of the copper loss is the majority of the total loss, the total loss barely increases. On the other hand, the torque of the designed motor increased by 16.7%, from 1.51 N·m to 1.75 N·m compared with that of the original motor. Therefore, the efficiency of the designed motor increased by 3.1%, from 77.4% to 80.5%. This is because the

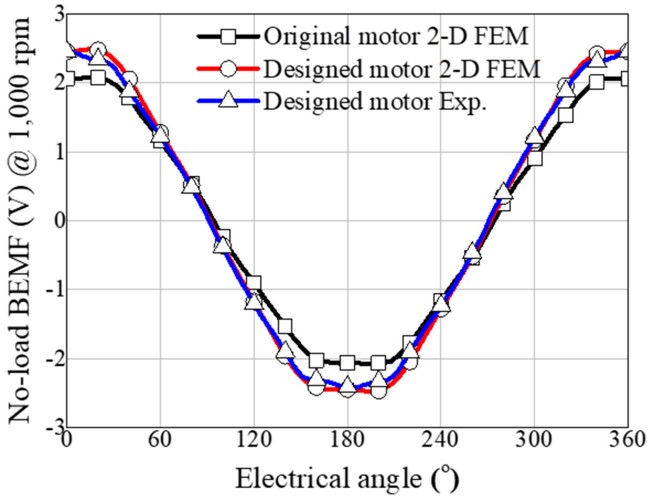

Fig. 15. Comparison of 2-D FEM simulation and no-load test BEMF.

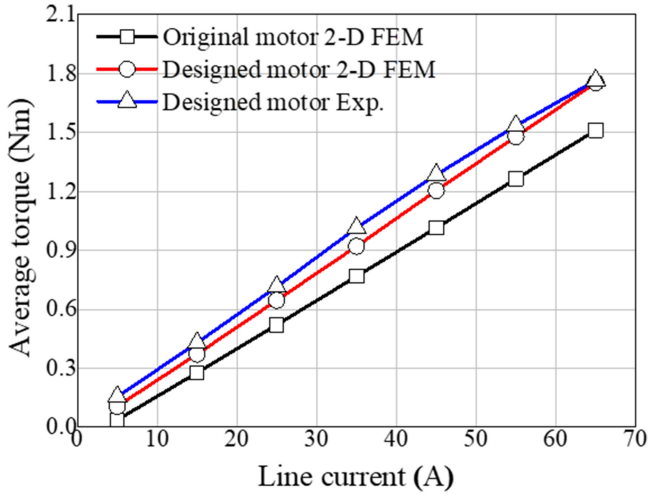

Fig. 16. Comparison of 2-D FEM and test results according to line current change.

TABLE IV
PERFORMANCE COMPARISON BETWEEN ORIGINAL AND DESIGNED MOTOR

Performance	Unit	Original motor	Designed motor
Power	W	522	605
Torque (@ 3,300 rpm)	Nm	1.51	1.75 (+16.7%)
Core loss	W	16	17
Copper loss	W	118	118
Efficiency	%	77.4	80.5 (+3.1%)

total loss was almost the same and the torque was improved compared with those of the original motor. This is shown in Table IV.

In conclusion, based on the above-mentioned results, it is confirmed that the torque improvement method and equivalent method proposed in this paper are valid.

V. CONCLUSION

In this paper, the design of the CFSM to improve torque methods are proposed. The thin pancake type CFSM covered in this paper has considerable axial magnetic leakage flux due to structural reasons. To meet the required specifications in a constrained installation space, this paper proposes two methods to improve both the torque and design process. The first method is the alternate-stacking core and this structure removes the magnetic leakage flux path. The second method is the rotor overhang and this structure increases the air-gap flux density. Although these methods have a 3-D magnetic field distribution, we have proposed and verified a method of equalizing the 3-D magnetic field distribution with the 2-D magnetic field distribution. This is done using the EMC to confirm the characteristics of the motor quickly and easily.

In conclusion, the motor using the method for improving the torque has improved about 10% of the torque compared to the original motor, while the FEM analysis result and the test result show an error of 0.6%. The efficiency of the designed motor increased by 3.1%, from 77.4% to 80.5%.

Therefore, it is confirmed that the torque improvement method and equivalent method proposed in this paper are valid.

REFERENCES

[1] T. Yamasaki, M. Eguchi, and Y. Makino, "Development of an electromechanical brake," NTN Corp., Japan, NTN Technical Review, no. 75, pp. 53–61, 2007. Available: http://www.ntnglobal.com/en/products/review/index.html

[2] C. Stancu, T. Ward, K. M. Rahman, R. Dawsey, and P. Savagian, "Separately excited synchronous motor with rotary transformer for hybrid vehicle application," *IEEE Trans. Ind. Appl.*, vol. 54, no. 1, pp. 223–231, Jan./Feb. 2018.

[3] M. S. Lim, J. M. Kim, Y. S. Hwang, and J. P. Hong, "Design of an ultra-high speed permanent magnet motor for an electric turbocharger considering speed response characteristics," *IEEE/ASME Trans. Mechatronics*, vol. 22, no. 2, pp. 774–784, Apr. 2017.

[4] L. Tang and G. J. Su, "High-Performance control of two three-phase permanent-magnet synchronous machines in an integrated drive for automotive applications," *IEEE Trans. Power Electron.*, vol. 23, no. 6, pp. 3047–3055, Nov. 2008.

[5] Y. H. Jung, M. S. Lim, M. H. Yoon, J. S Jeong, and J. P. Hong, "Torque ripple reduction of IPMSM applying asymmetric rotor shape under certain load condition," *IEEE Trans. Energy Convers.*, vol. 33, no. 1, pp. 333–340, Mar. 2018.

[6] J. H. Seo, S. M. Kim, and H. K. Jung, "Rotor-Design strategy of IPMSM for 42 V integrated starter generator," *IEEE Trans. Magn.*, vol. 46, no. 6, pp. 2458–2461, Jun. 2010.

[7] M. S. Lim, S. H. Chai, and J. P. Hong, "Design of saliency-based sensorless-controlled IPMSM with concentrated winding for EV traction," *IEEE Trans. Magn.*, vol. 52, no. 3, Mar. 2016, Art. no. 8200504.

[8] I. P. Brown *et al.*, "Design and evaluation of interior permanent-magnet compressor motors for commercial transcritical CO2 (R-744) heat pump water heaters," *IEEE Trans. Ind. Appl.*, vol. 51, no. 1, pp. 576–586, Jan./Feb. 2015.

[9] C. Xia, L. Guo, Z. Zhang, T. Shi, and H. Wang, "Optimal designing of permanent magnet cavity to reduce iron loss of interior permanent magnet machine," *IEEE Trans. Magn.*, vol. 51, no. 12, Dec. 2015, Art. no. 8115409.

[10] W. Ren, Q. Xu, Q. Li, and L. Zhou, "Reduction of cogging torque and torque ripple in interior PM machines with asymmetrical V-Type rotor design," *IEEE Trans. Magn.*, vol. 52, no. 7, Jul. 2016, Art. no. 8104105.

[11] W. Zhao, T. A. Lipo, and B. I. Kwon, "Torque pulsation minimization in spoke-type interior permanent magnet motors with skewing and sinusoidal permanent magnet configurations," *IEEE Trans. Magn.*, vol. 51, no. 11, Nov. 2015, Art. no. 8110804.

[12] J. M. Mun, G. J. Park, S. H. Seo, D. W. kim, Y. J. Kim, and S. Y. Jung, "Design characteristics of IPMSM with wide constant power speed range for EV traction," *IEEE Trans. Magn.*, vol. 53, no. 6, Jun. 2017, Art. no. 8105104.
[13] F. J. Lin, Y. T. Liu, and W. A. Yu, "Power perturbation based MTPA with an online tuning speed controller for an IPMSM drive system," *IEEE Trans. Ind. Electron.*, vol. 65, no. 5, pp. 3677–3687, May 2018.
[14] M. Obata, S. Morimoto, M. Sanada, and Y. Inoue, "Performance of PMASynRM with ferrite magnets for EV/HEV applications considering productivity," *IEEE Trans. Ind. Appl.*, vol. 50, no. 4, pp. 2427–2435, Jul./Aug. 2014.
[15] W. Zhao, D. Chen, T. A. Lipo, and B. I. Kwon, "Performance improvement of ferrite-assisted synchronous reluctance machines using asymmetrical rotor configurations," *IEEE Trans. Magn.*, vol. 51, no. 11, Nov. 2015, Art. no. 8108504.
[16] K. Sone, M. Takemoto, S. Ogasawara, K. Takezaki, and H. Akiy, "A ferrite PM In-Wheel motor without rare earth materials for electric city commuters," *IEEE Trans. Magn.*, vol. 48, no. 11, pp. 2961–2964, Nov. 2012.
[17] J. H. Park, Y. H. Jung, K. T. Jung, M. H. Yoon, and J. P. Hong, "Torque density improvement of concentrated flux-type synchronous motor for automotive application," in *Proc. IEEE Int. Elect. Mach. Drives Conf.*, 2017.
[18] S. I. Kim, J. Cho, S. Park, T. Park, and S. Lim, "Characteristics comparison of a conventional and modified spoke-type ferrite magnet motor for traction drives of low-speed electric vehicles," *IEEE Trans. Ind. Appl.*, vol. 49, no. 6, pp. 2516–2523, Nov./Dec. 2013.
[19] H. W. Kim, K. T. Kim, Y. S. Jo, and J. Hur, "Optimization methods of torque density for developing the neodymium free SPOKE-Type BLDC motor," *IEEE Trans. Magn.*, vol. 49, no. 5, pp. 2173–2176, May 2013.
[20] M. Barcaro and N. Bianchi, "Interior PM machines using ferrite to replace rare-earth surface PM machines," *IEEE Trans. Ind. Appl.*, vol. 50, no. 2, pp. 979–985, Mar./Apr. 2014.
[21] M. Fasil, N. Mijatovic, B. B. Jensen, and J. Holboll, "Performance variation of ferrite magnet PMBLDC motor with temperature," *IEEE Trans. Magn.*, vol. 51, no. 12, Dec. 2015, Art. no. 8115106.
[22] F. J. H. Kalluf, A. S. Isfanuti, L. N. Tutelea, A. Moldovan-Popa, and I. Boldea, "1-kW 2000–4500 r/min ferrite PMSM drive: Comprehensive characterization and two sensorless control options," *IEEE Trans. Ind. Appl.*, vol. 52, no. 5, pp. 3980–3989, Sep./Oct. 2016.
[23] S. J. Galioto, P. B. Reddy, A. M. EL-Refaie, and J. P. Alexander, "Effect of magnet types on performance of high-speed spoke interior-permanent-magnet machines designed for traction applications," *IEEE Trans. Ind. Appl.*, vol. 51, no. 3, pp. 2148–2160, May/Jun. 2015.
[24] S. G. Lee, J. Lee, and W. H. Kim, "A study on correcting the nonlinearity between stack length and back electromotive force in spoke type ferrite magnet motors," *IEEE Trans. Magn.*, vol. 53, no. 6, Jun. 2017, Art. no. 8201404.
[25] K. Wang, Z. Q. Zhu, and G. Ombach, "Torque enhancement of surface-mounted permanent magnet machine using third-order harmonic," *IEEE Trans. Magn.*, vol. 50, no. 3, Mar. 2014, Art. no. 8100210.
[26] W. Zhao, T. A. Lipo, and B. I. Kwon, "Dual-stator two-phase permanent magnet machines with phase-group concentrated-coil windings for torque enhancement," *IEEE Trans. Magn.*, vol. 51, no. 11, Nov. 2015, Art. no. 8112404.
[27] Z. Y. Gu, K. Wang, Z. Q. Zhu, Z. Z. Wu, C. Liu, and R. W. Cao, "Torque improvement in five-phase unequal tooth SPM machine by injecting third harmonic current," *IEEE Trans. Veh. Technol.*, vol. 67, no. 1, pp. 206–215, Jan. 2018.
[28] S. W. Hwang, J. H. Sim, J. P. Hong, and J. Y. Lee, "Torque improvement of wound field synchronous motor for electric vehicle by PM-assist," *IEEE Trans. Ind. Appl.*, vol. 54, no. 4, pp. 3252–3259, Jul./Aug. 2018.
[29] X. Ge, Z. Q. Zhu, J. Li, and J. Chen, "A spoke-type IPM machine with novel alternate airspace barriers and reduction of unipolar leakage flux by step-staggered rotor," *IEEE Trans. Ind. Appl.*, vol. 52, no. 6, pp. 4789–4797, Nov./Dec. 2016.
[30] K. C. Kim, D. H. Koo, and J. Lee, "The study on the overhang coefficient for permanent magnet machine by experimental design method," *IEEE Trans. Magn.*, vol. 43, no. 6, pp. 2483–2485, Jun. 2007.
[31] J. Y. Song, J. H. Lee, Y. J. Kim, and S. Y. Jung, "Computational method of effective remanence flux density to consider PM overhang effect for spoke-type PM motor with 2-D analysis using magnetic energy," *IEEE Trans. Magn.*, vol. 52, no. 3, Mar. 2016, Art. no. 8200304.
[32] J. H. Sim, D. G. Ahn, D. Y. Kim, and J. P. Hong, "Three-dimensional equivalent magnetic circuit network method for precise and fast analysis of PM-assisted claw-pole synchronous motor," *IEEE Trans. Ind. Appl.*, vol. 54, no. 1, pp. 160–171, Jan./Feb. 2018.

Jong-Hyun Park received the bachelor's degree in automotive engineering from Kookmin University, Seoul, South Korea, in 2014, and the master's degree in automotive engineering from Hanyang University, Seoul, South Korea, in 2018.

He is currently a Research Engineer with Hyundai Transys Co., Hwaseong, South Korea. His research interests include the design and analysis of traction motor for hybrid and electric vehicle powertrain systems.

Kyung-Tae Jung received the B.S. degree in mechanical engineering in 2011 from Hanyang University, Seoul, South Korea, where he is currently working toward the Ph.D. degree in automotive engineering.

His research interests include electric machine design for automotive applications, and numerical analysis of electromagnetic.

Young-Hoon Jung received the bachelor's degree in mechanical engineering in 2013 from Hanyang University, Seoul, South Korea, where he is currently working toward the Ph.D. degree in automotive engineering. His research interests include electric machine design for automotive and robot applications, and ultra-high speed motors.

Myung-Seop Lim received the bachelor's degree in mechanical engineering and the master's and Ph.D. degrees in automotive engineering from Hanyang University, Seoul, South Korea, in 2012, 2014, and 2017, respectively.

From 2017 to 2018, he was a Research Engineer with Hyundai Mobis, Yongin, South Korea. Since 2018, he has been with Yeungnam University, Gyeongbuk, South Korea, where he is currently an Assistant Professor. His research interests include electromagnetic field analysis and electric machinery for mechatronics systems, such as automotive and robot applications.

Myung-Hwan Yoon received the bachelor's degree in mechanical engineering and the master's and Ph.D. degrees in automotive engineering from Hanyang University, Seoul, South Korea, in 2011, 2013, and 2018, respectively.

Since 2018, he has been a Senior Research Engineer with Hyundai Motor Co., Ltd., Hwaseong, South Korea. His research interests include electromagnetic field analysis and electric machinery for automotive applications.

Jung-Pyo Hong (SM'97) received the Ph.D. degree in electrical engineering from Hanyang University, Seoul, South Korea, in 1995.

From 1996 to 2006, he was a Professor with Changwon National University, Changwon, South Korea. Since 2006, he has been a Professor with the Hanyang University. His research interests include the design of electric machines, optimization, and numerical analysis of electromechanics.

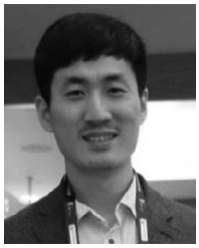

Jae-Woo Jung received the B.S. and M.S. degrees in electrical engineering from Changwon National University, Changwon, South Korea, in 2005 and 2007, respectively, and the Ph.D. degree in automotive engineering from Hanyang University, Seoul, South Korea, in 2013.

From 2009 to 2012, he developed PMSM for automotive application. Since 2013, he has been a Research Staff Member with the R&D center, Hyundai Mobis Co., Ltd., Yongin, South Korea. His research interests include the design and analysis of various electromagnetic devices for electromechanical brake system.